

Composition inversion in mixtures of binary colloids and polymer

Isla Zhang, Rattachai Pinchaipat, Nigel B. Wilding, Malcolm A. Faers, Paul Bartlett, Robert Evans, and C. Patrick Royall

Citation: [The Journal of Chemical Physics](#) **148**, 184902 (2018); doi: 10.1063/1.5023393

View online: <https://doi.org/10.1063/1.5023393>

View Table of Contents: <http://aip.scitation.org/toc/jcp/148/18>

Published by the [American Institute of Physics](#)

Articles you may be interested in

[The folding pathways and thermodynamics of semiflexible polymers](#)

The Journal of Chemical Physics **148**, 184901 (2018); 10.1063/1.5018114

[Communication: Glass transition and melting lines of an ionic liquid](#)

The Journal of Chemical Physics **148**, 171101 (2018); 10.1063/1.5030083

[Perspective: Outstanding theoretical questions in polymer-nanoparticle hybrids](#)

The Journal of Chemical Physics **147**, 020901 (2017); 10.1063/1.4990501

[Fluctuation-dissipation relation and stationary distribution of an exactly solvable many-particle model for active biomatter far from equilibrium](#)

The Journal of Chemical Physics **148**, 185101 (2018); 10.1063/1.5020654

[Perspective: Dissipative particle dynamics](#)

The Journal of Chemical Physics **146**, 150901 (2017); 10.1063/1.4979514

[Aging near rough and smooth boundaries in colloidal glasses](#)

The Journal of Chemical Physics **147**, 224505 (2017); 10.1063/1.5000445

PHYSICS TODAY

WHITEPAPERS

ADVANCED LIGHT CURE ADHESIVES

READ NOW

Take a closer look at what these
environmentally friendly adhesive
systems can do

PRESENTED BY



Composition inversion in mixtures of binary colloids and polymer

Isla Zhang,^{1,2} Rattachai Pinchaipat,^{2,3} Nigel B. Wilding,⁴ Malcolm A. Faers,⁵ Paul Bartlett,¹ Robert Evans,³ and C. Patrick Royall^{1,2,3}

¹School of Chemistry, Cantock's Close, University of Bristol, Bristol BS8 1TS, United Kingdom

²Centre for Nanoscience and Quantum Information, Bristol BS8 1FD, United Kingdom

³HH Wills Physics Laboratory, University of Bristol, Bristol BS8 1TL, United Kingdom

⁴Department of Physics, University of Bath, Bath BA2 7AY, United Kingdom

⁵Bayer AG, Alfred Nobel Str. 50, 40789 Monheim, Germany

(Received 23 January 2018; accepted 19 April 2018; published online 9 May 2018)

Understanding the phase behaviour of mixtures continues to pose challenges, even for systems that might be considered “simple.” Here, we consider a very simple mixture of two colloidal and one non-adsorbing polymer species, which can be simplified even further to a size-asymmetrical binary mixture, in which the effective colloid-colloid interactions depend on the polymer concentration. We show that this basic system exhibits surprisingly rich phase behaviour. In particular, we enquire whether such a system features only a liquid-vapor phase separation (as in one-component colloid-polymer mixtures) or whether, additionally, liquid-liquid demixing of two colloidal phases can occur. Particle-resolved experiments show demixing-like behaviour, but when combined with bespoke Monte Carlo simulations, this proves illusory, and we reveal that only a single liquid-vapor transition occurs. Progressive migration of the small particles to the liquid phase as the polymer concentration increases gives rise to *composition inversion*—a maximum in the large particle concentration in the liquid phase. Close to criticality, the density fluctuations are found to be dominated by the larger colloids. Published by AIP Publishing. <https://doi.org/10.1063/1.5023393>

I. INTRODUCTION

It is difficult to overstate the importance of mixtures as they constitute the vast majority of materials. The most basic mixtures are those of two species, and studies of such binary atomic and molecular mixtures have a distinguished history. In particular, much is known about the topologies of their possible phase diagrams from a theoretical perspective.^{1,2} However, experimental studies of such systems do not generally provide detailed information on central features such as the compositions and structure of coexisting phases, the character of near-critical fluctuations, and the link between the form of the microscopic interactions and the phase behavior. In this respect, colloidal dispersions are versatile systems for gaining insight into these basic aspects of phase behaviour.^{3,4}

Adding non-adsorbing polymer depletant induces entropically driven attraction between colloidal particles, and such mixtures can be interpreted as colloidal systems with the polymer degrees of freedom *integrated out*. Because the resulting colloid-colloid interactions are very similar to those of atoms and molecules, these systems likewise exhibit fluid, liquid, and crystalline phases, along with metastable states such as glasses and gels.^{5,6} A key advantage over atomic and molecular systems is that one can readily modify the strength and range of the effective particle interactions while directly observing the structure at the particle-resolved level using microscopy.⁴

Although colloid-polymer mixtures have proven invaluable in elucidating the properties of single-component

fluids,^{5,7,8} surprisingly, little attention has been given to binary colloidal mixtures (plus polymer depletant). Investigations to date include sedimentation profiles, where kinetics and equilibrium phase behaviour can exhibit a complex interplay,^{9–11} and studies of dynamics, where electrostatic interactions lead to non-intuitive behavior.¹² Studies of phase behaviour indicate a time-dependent stratification of the sediment into layers with differing composition.^{10,11} We note that complex behaviour can occur under a gravitational field,^{13–16} and it is uncertain whether the stratification observed in Refs. 10 and 11 is thermodynamic or gravitational in origin.

The current theoretical understanding of such mixtures remains relatively little developed. One important result is that the free-volume approach of Lekkerkerker *et al.*¹⁷ can be generalised to the present ternary mixture of two colloid species and polymer and predicts only vapor-liquid coexistence for the parameters of our experiments.¹⁸ Here, we report a combined experimental and simulation study of the phase behavior of a binary colloid mixture with a single species of added polymer. We describe the system in terms of an effective binary colloidal mixture in which the explicit polymer degrees of freedom are integrated out: colloidal interactions then take a form that is parameterized in terms of a polymer reservoir mass fraction c_p^r that plays the role of inverse temperature. Central questions concern (i) the topology of the phase diagram of such a system and (ii) the structure and composition of the coexisting phases.

As the effective interactions between colloids resemble those found for binary mixtures of simple atomic fluids, we

might expect to find phase behaviour similar to that proposed previously on the basis of mean field theories of a van der Waals mixture. Reference 2 identified several classes of possible phase diagram topology, which were subsequently found to apply to a wide range of real atomic and molecular mixtures.¹ The classes are delineated by the degree of immiscibility of the two components. For mixtures in which the two species are not too dissimilar, one of two scenarios is predicted: For type I behavior, the system exhibits only liquid-vapor phase separation, which for our case would correspond to coexistence between a colloid-rich “liquid” phase (dilute in polymer) and a polymer-rich “vapor” phase (dilute in colloids). Type II phase diagrams occur when the immiscibility is stronger: following liquid-vapor phase separation, a further transition occurs at sufficiently large c_p^r (low effective temperature) corresponding to a deep quench in which liquid-liquid demixing occurs at a critical end point, with a line of demixing critical points extending to higher densities. Below a critical end point, two liquids—one rich in the larger colloids and the other in the small colloids—coexist with a vapor phase. Possible scenarios are sketched in the second row of Fig. 1.

Although there are basic similarities with simple atomic mixtures, the colloidal system we study exhibits key differences: (i) the ratio of the colloid diameters, 0.57, is rather large and (ii) unlike atomic mixtures the range of all three attractive (colloid-colloid) pair interactions is identical since this is

set by the size of the single polymer species. Moreover, the well depth of the effective depletion attraction between two large particles is about twice that between two small particles. Thus, it is not clear *a priori* which scenario for the fluid phase separation, type I or type II, should pertain in our system. It is also conceivable that, given that the interaction between the large colloids is stronger than that between the small colloids, the former might demix with the small acting in a similar way to a “spectator phase.” Furthermore, at sufficiently large c_p^r , colloids can undergo gelation, which is not foreseen in the classification scheme.² Remarkably, we find that in our experiments, the system appears to exhibit three-phase coexistence. However, careful analysis informed by simulation reveals that this is illusory: there are two phases, yet their composition changes so drastically that it gives the impression of a new phase. We choose to term this non-monotonic behaviour of the ratio of volume fractions *composition inversion*.

To understand this basic mixture, we combine particle-resolved experiments⁴ with tailored Grand Canonical Ensemble (GCE) Monte Carlo (MC) simulation.¹⁹ Our experiments use confocal microscopy to provide real-space information on composition fluctuations and fractionation effects. These characterize phase coexistence and criticality in colloidal binary mixtures. Our system consists of two species, i.e., two sizes of fluorescently labelled colloidal particles that are (nearly) density- and refractive index-matched to their solvent. To this

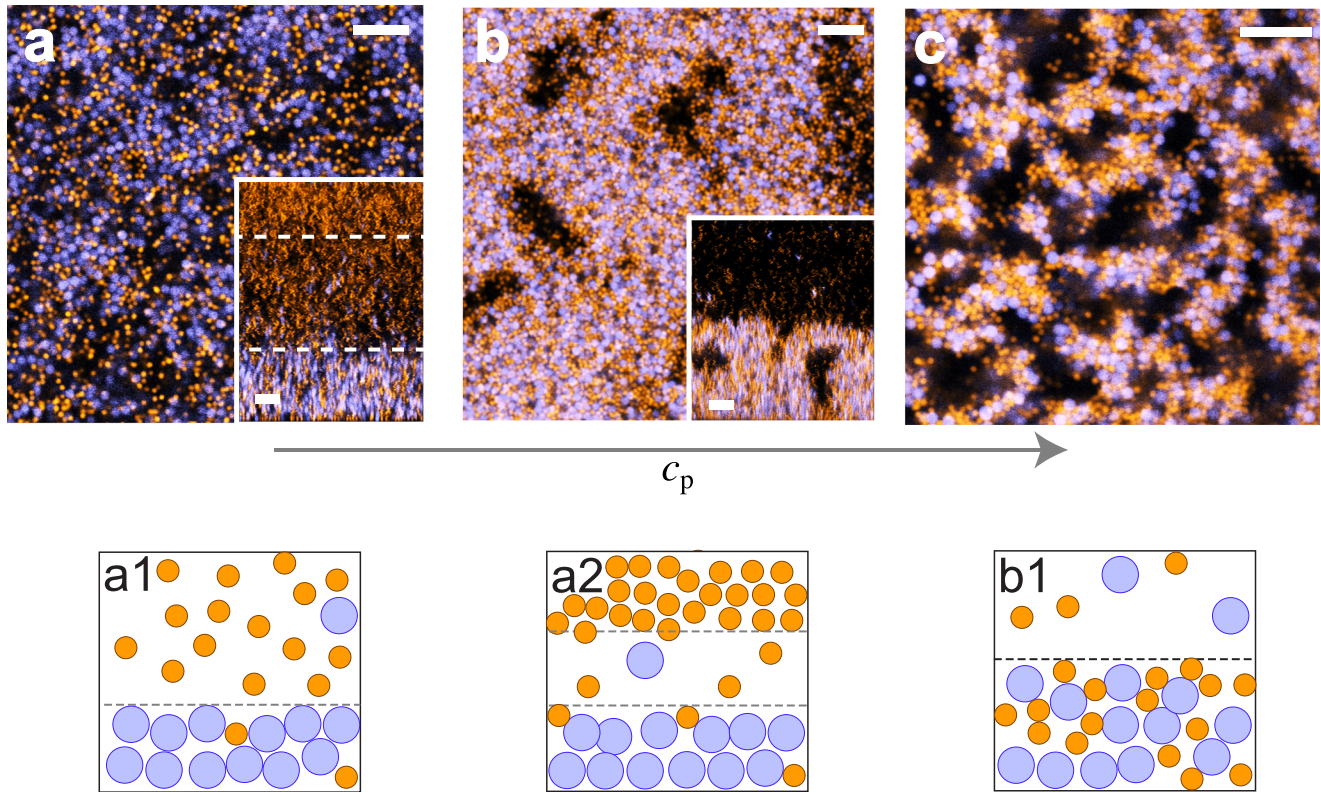


FIG. 1. Phase behaviour of binary colloid-polymer mixtures. [(a)-(c)] Confocal microscopy images (see text) with large (blue) and small (orange) colloids. Insets show xz profiles that are $100 \mu\text{m}$ in height. (a) $c_p/c_p^* = 0.059$, possible two- or three-phase demixing as indicated by dashed lines in the inset; (b) $c_p/c_p^* = 0.069$; (c) $c_p/c_p^* = 0.090$, gelation. Scale bars denote $10 \mu\text{m}$. Possible scenarios by which the experimental data may be interpreted: (a1) Two-phase coexistence—the lower (liquid) phase is rich in large particles and the upper (vapor) phase is rich in small particles and polymer; (a2) The colloidal mixture exhibits liquid-liquid demixing; (b1) Upon deeper quenching, more small particles become entrained in the colloid-rich liquid.

system, polymer is added. Our simulations provide comparable information but are free from the influence of kinetics and gravity; they access equilibrium properties. In particular, we obtain densities of coexisting phases and their spatial fluctuations. In our simulations, the effective colloid-colloid interactions are described by the Asakura-Oosawa (AO) model^{20,21} generalised to a binary system.

This paper is organised as follows. In the Methods section (Sec. II), we discuss our experimental procedure in Sec. II A and the way in which we map our data between experiment and simulation is described in Sec. II B. The means we use to arrive at an effective Hamiltonian for the binary colloid system are described in Sec. II C, and our tailored simulation methodology is introduced in Sec. II D. In the Results section (Sec. III), we describe the single-component colloid-polymer phase behaviour in Sec. III A before proceeding to the phase behavior of the binary colloids plus polymer, which is the main experimental result of this work in Sec. III B. Simulation results for the phase behaviour are presented in Sec. III C. Our finding of composition inversion is discussed in Sec. III D, and we complete our results section by showing the behaviour of near-critical fluctuations in Sec. III E. We conclude our paper in Sec. IV.

II. METHODS

A. Experimental details

Two sizes of poly(methylmethacrylate) (PMMA) particles were used. Using static light scattering, the diameters of the large l and small s particles were determined to be $\sigma_l = 1.84 \mu\text{m}$ and $\sigma_s = 1.04 \mu\text{m}$, respectively, with polydispersity of 5% in each case. The colloid-colloid size ratio is then $q_{sl} = 0.57$. The larger particles were labeled with the fluorescent dye 3,3-dioctadecyloxacarbocyanine perchlorate (DiOC₁₈), while the smaller particles were labeled with 1,1-dioctadecyl-3,3,3,3-tetramethylindocarbocyanine perchlorate (DiIC₁₈). The solvent used was a mixture of tetrachloroethylene and *cis*-decalin, which closely matched the refractive indices and densities of the two colloid species. The colloids were produced in two separate syntheses, and consequently, their mass density was slightly different. As a result, it is not possible to completely density-match both the species, and indeed, the solvent density lies between that of the two species such that one creams and one sediments. However, close density matching for colloids of this size leads to gravitational lengths in excess of 10 particle diameters;²² so, we conclude that gravity has a small effect on the behavior we observe. Polystyrene with molecular weight $m_w = 1.5 \times 10^7 \text{ g mol}^{-1}$ acted as the depletant, with radius of gyration $R_g \approx 149 \text{ nm}$ in the good solvent used,²³ giving polymer-colloid size ratios of $q_l = 2R_g/\sigma_l = 0.16$ and $q_s = 2R_g/\sigma_s = 0.29$ for the large and the small particles, respectively. The sizes of the particles and the depletant were chosen such that a stable colloidal liquid should exist for the mixture with only smaller particles, while in the case of the larger particles, the liquid is metastable to crystallization.^{5,6}

We work in the vicinity of the critical isochore. For each pure colloid species l and s , the critical colloid volume frac-

tion was estimated from the literature^{8,24–26} to be $\phi_l^c = 0.26$ and $\phi_s^c = 0.22$, respectively. For the mixture, an intermediate total overall volume fraction of $\phi_{tot} \equiv \phi_s + \phi_l = 0.24$ was chosen, with $\phi_s = \phi_l$, implying that the overall concentration of large particles is $X_l \equiv N_l/(N_s + N_l) = 0.143$. We focus on state points along this isochore distinguished by the choice of polymer mass fraction c_p . Since colloid-polymer mixtures have large critical regimes with relatively flat binodals, a precise determination of the critical isochore is not essential for the purposes of observing near-critical fluctuations.⁸ When plotting experimental results, we use the ratio c_p/c_p^* , where c_p^* is the value at overlap.

Phase diagrams in the experiments are determined as follows. In single-phase regions (one-phase fluid or gel), we quote the colloid volume fraction at which the sample is prepared. In the case of phase separation, a sedimentation profile is used to determine the volume fraction of each colloid species as a function of height.

Sedimentation profiles were obtained from an intensity analysis that was calibrated using images of samples having known volume fraction. The fraction of the total intensity due to each species is nearly linearly dependent on the volume fraction of that species.⁹ Given the calibration, we then determine the volume fraction as a function of position. Specifically, the volume fractions of both colloid species $\phi_i(x, y, z)$ where $i = l, s$ were calculated from an intensity average fraction around the point (x, y, z) , i.e.,

$$\phi_i(x, y, z) \approx C \frac{\sum_{x=-L_x}^{L_x} \sum_{y=-L_y}^{L_y} \sum_{z=-L_z}^{L_z} I_i(x, y, z)}{8I_{\max} N_x N_y N_z}, \quad (1)$$

where $C \approx 1 \pm 0.012$ is a calibration constant and N_x, N_y, N_z are the number of pixels in $[-L_j, L_j]$. In our case, L_i is selected to be $7.0\sigma_l$ as in the simulations and $j \in \{x, y, z\}$. $I_{\max} = 255$ is the maximum intensity, scaled by 8 to reflect the two channels. The sedimentation profile was obtained by scanning the xy plane at every z position.

B. Mapping experiment to simulation

As noted above, our experimental results are plotted in terms of the dimensionless ratio c_p/c_p^* , where c_p^* is the polymer mass fraction at overlap and c_p refers to the polymer mass fraction in the actual (experimental) polymer-colloid mixture. On the other hand, models and simulations of such mixtures are most naturally formulated in terms of a polymer reservoir, with a given chemical potential μ_p , which is in osmotic equilibrium with the actual system. One can convert from the reservoir to the system representation if one knows the free volume fraction $\alpha(\phi_l, \phi_s; z_p)$ that relates the number density of polymers in the system to that in the reservoir ρ_p^r :

$$\rho_p(\phi_l, \phi_s; z_p) = \alpha(\phi_l, \phi_s; z_p) \rho_p^r(z_p), \quad (2)$$

where z_p is the fugacity of the polymer. Free volume arguments suggest that the free volume fraction can be approximated by its value in the limit $z_p \rightarrow 0$, i.e., vanishing polymer density. Within the context of the Asakura-Oosawa model, where the polymer is ideal and $z_p = \rho_p^r$ (see Subsection II C), the

free volume fraction is easily calculated from Percus-Yevick (PY) results, equivalent to scaled particle theory, for the excess chemical potential of a binary hard-spheres (HS) mixture.^{17,27} We have generalized this approach to the ternary HS case, and within the PY approximation, we find the following result in the limit $z_p \rightarrow 0$:

$$\alpha^{PY}(\phi_l, \phi_s; z_p = 0) = (1 - \phi_{\text{tot}}) \exp[-\tilde{A}\tilde{\gamma} - \tilde{B}\tilde{\gamma}^2 - \tilde{C}\tilde{\gamma}^3], \quad (3)$$

where

$$\tilde{\gamma} = \frac{1}{1 - \phi_{\text{tot}}}, \quad (4)$$

$$\tilde{A} = \phi_l q_l^3 + \phi_s q_s^3 + 3(\phi_l q_l^2 + \phi_s q_s^2) + 3(\phi_l q_l + \phi_s q_s), \quad (5)$$

$$\tilde{B} = \frac{9}{2}(\phi_l q_l + \phi_s q_s)^2 + 3(\phi_l q_l^2 + \phi_s q_s^2)(\phi_l q_l + \phi_s q_s), \quad (6)$$

and

$$\tilde{C} = 3(\phi_l q_l + \phi_s q_s)^3. \quad (7)$$

In the limit where the volume fraction of one colloid species vanishes, this result reduces to that of Lekkerkerker *et al.*¹⁷ For our experimental conditions, $q_l = 0.16$, $q_s = 0.29$, $\phi_l = \phi_s = 0.12$, we find that this approximation gives a free volume fraction $\alpha^{PY} \sim 0.6$. Theory and simulation for the AO model usually work with the polymer reservoir volume fraction $\phi_p^r = \pi \sigma_p^3 \rho_p^r / 6$. This quantity sets the strength of the attractive interactions [see Eq. (12) and Fig. 3]. For example, our simulations yield a critical point at $\phi_p^r = 0.375(5)$. In the text, we use the term c_p^r , the polymer reservoir concentration, to denote ϕ_p^r . Since for fixed ϕ_l and ϕ_s , α^{PY} in (3) is constant, it follows that to a good approximation we can convert from simulation to experiment assuming $c_p/c_p^* \propto \phi_p^r$. We fix the constant by matching the critical points in simulation and experiment. We estimate the experimental critical point to be at $c_p/c_p^* = 0.057 \pm 0.002$ [see Fig. 5(ii)]. There is a small deviation from linearity (<5%) upon phase separation. Although we could correct for this using the appropriate colloid volume fractions in α^{PY} , this would not remove other errors in the mapping. These arise from polymer non-ideality, deformation, and other deviations from the ideal AO model.^{28–31}

C. The effective two-component Hamiltonian

In this subsection, we describe the model that we investigate in simulations. We consider a ternary system consisting of two species of colloids, modelled as large and small hard-spheres (HS) with different diameters σ_l , σ_s , plus a single polymer species p . The Hamiltonian is

$$H = H_{ll} + H_{ss} + H_{ls} + H_{lp} + H_{sp} + H_{pp}, \quad (8)$$

where H_{ll} denotes hard sphere (HS) interactions between ll , H_{ss} denotes HS interactions between ss , and H_{ls} denotes HS interactions between unlike species. The ls HS interaction potential $u_{ls}^{HS}(r)$ is assumed additive so that the cross-diameter $\sigma_{ls} \equiv (\sigma_l + \sigma_s)/2$. The polymer coils are treated as mutually interpenetrable (non-interacting or ideal) so that $H_{pp} = 0$. However, the centre of mass of a coil is excluded from the large colloid centre to a distance $(\sigma_l + \sigma_p)/2$ or $(\sigma_s + \sigma_p)/2$ for the small colloid. The diameter of the polymer is

$\sigma_p = 2R_g$, where R_g is the radius of gyration of the polymer. Equation (8) defines the Asakura-Oosawa (AO) model for our present ternary mixture.^{20,21,32} Henceforward, we ignore trivial kinetic energy terms.

Following Ref. 27, we work in the semi-grand ensemble where the numbers N_l and N_s of the large and small HS, respectively, are fixed, as are the volume V , inverse temperature β , and the polymer fugacity $z_p = \Lambda_p^{-3} \exp(\beta \mu_p)$. Here, Λ_p is the thermal de Broglie wavelength and μ_p is the chemical potential of the polymer reservoir. For ideal polymer, we recall $z_p = \rho_p^r$, the polymer density in the reservoir. The thermodynamic potential F appropriate to this ensemble is given by a direct generalization of Eq. (3) in Ref. 27, and the effective Hamiltonian of the two-component colloid mixture, obtained by integrating out the polymer degrees of freedom, takes the form

$$H^{\text{eff}} = H_{ll} + H_{ss} + H_{ls} + \Omega, \quad (9)$$

where Ω is the grand potential of the fluid of ideal polymer in the field of a fixed configuration of N_l and N_s HS colloids. Ω depends on the coordinates of both the HS species.²⁷

Extending the analysis presented in Ref. 27 to the binary HS case leads directly to a diagrammatic expansion of Ω , which generalizes Eq. (6) of Ref. 27; i.e., Ω is a sum of zero, one-body, two-body, and higher body colloidal terms that involve integrals over products of lp and sp Mayer bonds. The upshot is that the effective Hamiltonian takes the form:

$$H^{\text{eff}} = H_0 + \sum_{i < j}^{N_l} u_{ll}^{\text{eff}}(R_{ij}) + \sum_{i < j}^{N_s} u_{ss}^{\text{eff}}(R_{ij}) + \sum_{i=1}^{N_l} \sum_{j=1}^{N_s} u_{ls}^{\text{eff}}(R_{ij}) + \text{H.O. terms}, \quad (10)$$

where R_{ij} is the distance between the centres of particles i and j and the effective ll (or ss) pair potential u^{eff} is that pertaining to a one-component HS l (or s) AO system with the appropriate HS diameter σ_l (or σ_s).²⁷ The new two-body term is the effective ls pair potential that we write out explicitly below. The first term in Eq. (10) is the sum of zero and one-body term which, for a uniform mixture with constant densities, is

$$\beta H_0 = -z_p V \left[1 - \phi_l (1 + q_l)^3 - \phi_s (1 + q_s)^3 \right], \quad (11)$$

where $\phi_l = \pi \rho_l \sigma_l^3 / 6$, with number density $\rho_l = N_l / V$, is the volume fraction of the large (l) HS and equivalently for s . As noted earlier, the size ratios are $q_l = \sigma_p / \sigma_l$, $q_s = \sigma_p / \sigma_s$. Since H_0 / V depends linearly on ρ_l and ρ_s , this term does not affect the phase equilibria,²⁷ which is the concern of the present study. The higher order terms in (10) correspond to 3-body, 4-body, etc., effective inter-colloidal interactions. Generally, these terms are non-zero and, as the size ratios increase, we expect an increasing number of higher body contributions. However, for a sufficiently asymmetric case, i.e., with $q_s < (2/\sqrt{3} - 1) = 0.1547$ and following arguments of Ref. 27, it is easy to show that three- and higher body terms vanish identically in (10). Thus, in this regime, pair potentials alone determine phase equilibria, equilibrium distribution functions, and probability distribution functions (pdf). This is

an important result. It implies that for sufficiently asymmetric cases, the ternary AO system can be mapped *exactly* to a two-component colloid mixture in which the colloids interact solely through pair potentials. We return to this observation below.

$$\beta u_{ls}^{\text{eff}}(r) = \beta u_{ls}^{\text{HS}}(r) + \beta u_{ls}^{\text{AO}}(r) = \begin{cases} \infty, & 0 < r < \sigma_{ls} \\ \frac{\phi_p^r}{\sigma_p^3} \frac{(\sigma_{ls} + \sigma_p - r)^2 [3(\sigma_l - \sigma_s)^2 - 8r(\sigma_{ls} + \sigma_p) - 4r^2]}{8r}, & \sigma_{ls} < r < \sigma_{ls} + \sigma_p \\ 0, & r > \sigma_{ls} + \sigma_p \end{cases}, \quad (12)$$

where r is the distance between the centres of colloid l and colloid s and $\phi_p^r = \pi \rho_p^r \sigma_p^3 / 6$ is the volume fraction of the polymer in the reservoir. It is straightforward to show that (12) reduces to the standard one-component AO result when $\sigma_l = \sigma_s = \sigma_{ls}$.²⁷ The three effective pair potentials $u_{ll}^{\text{eff}}(r)$, $u_{ss}^{\text{eff}}(r)$, and $u_{ls}^{\text{eff}}(r)$ have different hard-core diameters but exhibit identical finite range of attraction, equal to σ_p , the diameter of the single polymer species. These pair potentials, employed in our computer simulations, are each proportional to ϕ_p^r , which implies that this quantity plays the same role as does inverse temperature in simple atomic fluids. A plot of the potentials, divided by ϕ_p^r , is given in Fig. 3 for the experimental size ratios $q_l = 0.16$ and $q_s = 0.29$. For these parameters, the depth of the ll depletion potential is about 1.7 times the ss depth, while the ls depth is about 1.24 times the ss depth. Note that these pair potentials are somewhat different from those one might choose to model a binary mixture of atomic fluids, say Xe and Ar. In our case, the range of the interaction is identical for all these pair potentials, whereas for the atomic case the range increases with the size and polarizability of the species.¹

Although the value of q_l we employ is only very slightly greater than 0.1547, i.e., the value where three-body contributions begin to contribute, q_s is considerably larger. This implies that in mapping the ternary AO model, for these particular parameters, to the effective two-component mixture, some many-body interactions are omitted. One can estimate the importance of the latter by considering the mapping of the standard AO model with species s only. For $q_s = 0.29$, the pair potential description provides an accurate description of the full binary AO mixture.³³

D. Tailored simulation methods

We employ grand canonical ensemble (GCE) Monte Carlo simulation to study a binary mixture of particles interacting

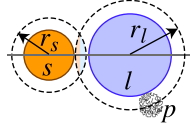


FIG. 2. Geometry for depletion interaction between unlike colloids l and s due to polymer p . The radius of the depletion sphere around l is $(\sigma_l + \sigma_p)/2$ and that around s is $(\sigma_s + \sigma_p)/2$. The overlap lens shape is indicated; its volume determines the depletion potential given in Eq. (12).

It remains to specify the ls effective pair potential. This is easily calculated. The attractive depletion or AO potential $u_{ls}^{\text{AO}}(r)$ is equal to the volume of the lens formed by the overlap of depletion layers around l and s times $-\zeta_p \beta^{-1}$. The geometry of the overlap is illustrated in Fig. 2. We find:

via the AO potential of u_{ll}^{eff} , u_{ss}^{eff} and u_{ls}^{eff} entering Eq. (10) with $q_l = 0.16$ and $q_s = 0.29$. Use of the GCE allows accurate and efficient simulation of fluid phase transitions and critical phenomena because it provides for density fluctuations on the scale of the simulation box. Traditional approaches of MD simulation in the microcanonical or canonical ensembles, while more straightforward to implement, lead to accuracy problems and, particularly for fluid mixtures, to enhanced finite-size effects.³⁴ Our approach is tailored to exploit the accuracy and flexibility of the GCE while simultaneously adhering to the experimental conditions of fixed overall volume fractions of the two components: $\phi_l = \phi_s = 0.12$. The challenge is to satisfy this global constraint on average, even when the system has separated into m coexisting phases, each occupying a certain proportion of the total volume. Under these conditions, the coexisting phases are generally “fractionated”; i.e., their compositions differ from one another and one should like to determine the composition of each phase and the fraction of the system that it occupies.

To see how this can be achieved, consider the distribution of particles between the phases. This is described by a generalized lever rule:

$$\phi_l^{(0)} = \sum_{\gamma=1}^m \xi^{(\gamma)} \phi_l^{(\gamma)}, \quad (13)$$

$$\phi_s^{(0)} = \sum_{\gamma=1}^m \xi^{(\gamma)} \phi_s^{(\gamma)}. \quad (14)$$

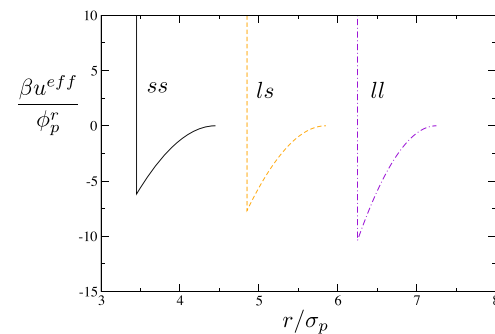


FIG. 3. The three effective pair potentials $\beta u^{\text{eff}}(r)$ plotted versus r/σ_p for size ratios $q_l = 0.16$ and $q_s = 0.29$. Note that the range of the attraction is σ_p for all the three potentials.

Here, $\phi_l^{(0)} = N_l \sigma_l^3 / (6V)$, $\phi_s^{(0)} = N_s \sigma_s^3 / (6V)$ are the overall (global) volume fractions of the two species l and s ; $\xi^{(\gamma)}$, $\gamma = 1, \dots, m$ is the phase fraction of phase γ , which satisfies $\sum_{\gamma=1}^m \xi^{(\gamma)} = 1$; $\phi_l^{(\gamma)}, \phi_s^{(\gamma)}$ are the volume fractions of the individual components in phase γ . It follows that in order to specify the coexistence properties of the system for some prescribed $\phi_s^{(0)}$ and $\phi_l^{(0)}$, one must determine $\xi^{(\gamma)}, \phi_s^{(\gamma)}, \phi_l^{(\gamma)}$ for each phase γ . This can be done iteratively within a histogram reweighting framework, using a variant of an approach originally developed in the context of polydisperse fluids.³⁵ Specifically, for given $\phi_s^{(0)}, \phi_l^{(0)}$ and ϕ_p^r , one regards the chemical potentials μ_s and μ_l and the phase fractions $\xi^{(\gamma)}$ as parameters to be tuned such as to satisfy both the generalized lever rule Eqs. (13) and (14) and equality of the probability of the phases. For this purpose, it is expedient to define a suitable order parameter probability distribution function (pdf), such as a density or composition distribution, which exhibits distinct peaks, one for each phase. The equality of the peak weights determines the conditions for which the phases are equally probable, which within the GCE implies that the phases have equal pressure. Additionally, the peaks in the pdf allow one to assign any given configuration to a phase on the basis of its order parameter. This in turn permits the ready determination of the ensemble-averaged volume fractions $\phi_s^{(\gamma)}$ and $\phi_l^{(\gamma)}$, which appear in the lever rule. Since the order parameter pdf typically exhibits large probability barriers corresponding to mixed phase states, its form is best determined using multicanonical preweighting.^{19,34}

Use of this method allows $\xi^{(\gamma)}, \phi_s^{(\gamma)}, \phi_l^{(\gamma)}$ to be determined with finite-size errors that are exponentially small in the system size.³⁵ This is true even if the prescribed coexistence state point lies close to the phase boundary, i.e., close to one end of a coexistence tie line, where the phase fraction of one phase vanishes. Standard methods for determining phase coexistence properties struggle in this regime because the minority phase contains very few particles. In our method, however, the phases that occur near the end of the coexistence tie line are instead studied under conditions corresponding to the center of the tie line. Here, the system fluctuates with equal probability between configurations in which each phase fills the simulation box in turn. This minimizes finite-size effects, while application of the lever rule condition allows us to infer accurately the phase fractions corresponding to the state point of interest close to the phase boundary. We note that our approach is more powerful and accurate than the Gibbs Ensemble MC method for obtaining phase behaviour of fluid mixtures, as discussed in Ref. 19.

III. RESULTS

A. Phase behavior of single colloid species-polymer mixtures: Experiment

We begin by noting the phase behavior of mixtures consisting of a single colloid species and polymer. For a sample comprising solely of large particles at the estimated critical colloid volume fraction of $\phi_l^c = 0.26$, liquid-vapor phase separation occurs at $c_p^c/c_p^* = 0.055 \pm 0.005$; likewise, for a sample comprising solely of small particles at the estimated critical

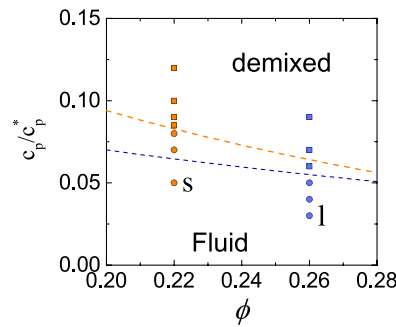


FIG. 4. Phase diagrams of colloid-polymer mixtures with one species of colloids. Orange data points are for the small particles ($q_s = 0.29$), with critical volume fraction $\phi_s^c = 0.22$. Blue data points are for the larger particles ($q_l = 0.16$), with critical volume fraction $\phi_l^c = 0.26$. Squares indicate phase coexistence or gelation; circles indicate a one-phase fluid. The dashed lines indicate purported phase boundaries ascertained from confocal images taken at various state points.

volume fraction of $\phi_s^c = 0.22$, phase separation occurs at $c_p^c/c_p^* = 0.0825 \pm 0.0025$. The phase boundaries for both the systems are indicated in Fig. 4.

B. Phase behavior of binary colloid-polymer mixtures: Experiment

The bidisperse colloid mixture undergoes phase separation at $c_p^c/c_p^* = 0.057 \pm 0.002$, indistinguishable from the system of large particles only. Confocal images in the xy plane at height z near the bottom of the container are shown in Fig. 1. The insets show the system in the xz plane. Consider first Fig. 1(a) that is for $c_p/c_p^* = 0.059$, corresponding to a shallow quench to a state point just within the phase coexistence region. The inset shows separation into two (or possibly three—see later) phases, the denser of which has sedimented. The upper phase is overwhelmingly composed of small particles (orange), while the lower phase contains the vast majority of the large particles (blue). However, the main panel reveals substantial numbers of small particles in the dense phase as well as significant spatial density fluctuations. On performing a deeper quench to $c_p/c_p^* = 0.069$ [Fig. 1(b)], one finds very different structure. From the inset, one observes phase separation with the denser phase sedimenting, but now there are many more small particles in the lower phase and very few in the upper phase. Finally, upon further quenching to $c_p/c_p^* = 0.090$ [Fig. 1(c)], the system undergoes dynamical arrest and a gel forms. Both species occupy the dense interpenetrating arms of the gel. A schematic phase diagram based on the analysis of these images is given in Fig. 5(iii).

Despite the particle-level detail, the results of Fig. 1 do not readily permit one to distinguish between type I and II phase behaviour. Specifically, Fig. 1(a) could be interpreted in a number of ways. The observation that the small colloids are fairly uniformly distributed among the phases could be taken to imply that the large colloids are somehow behaving as an effective one-component system that has undergone liquid-vapor phase separation, while the small particles only “spectate” in this process. Alternatively, it might be more appropriate to think in terms of the mixture as a whole undergoing liquid-vapor phase separation but with a strong fractionation of the large particles to the liquid phase and only weak fractionation

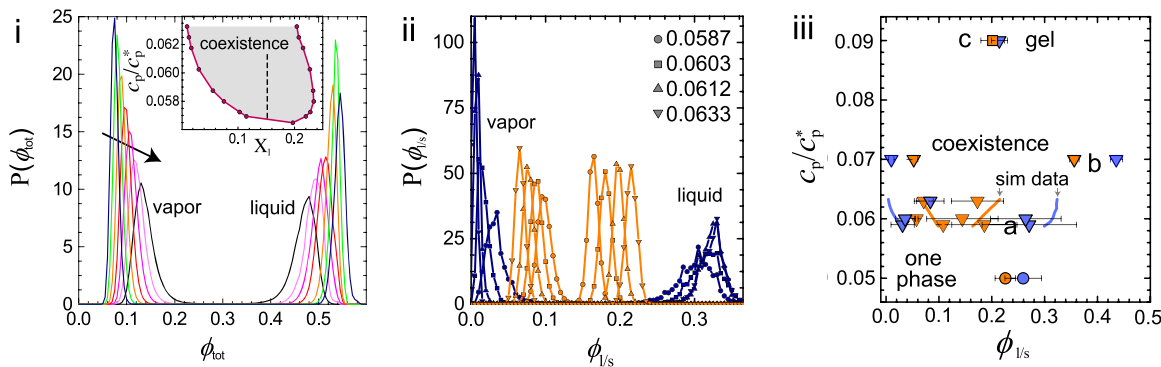


FIG. 5. (i) Grand Canonical Monte Carlo simulation results for the probability distribution $P(\phi_{\text{tot}})$ in the vapor and liquid phases for various polymer reservoir concentrations c_p^r . The arrow denotes reducing c_p^r and mapping to $c_p/c_p^* = 0.0633$ to equal increments. The inset shows the large particle concentration X_l in the vapor and liquid phases, with the overall composition $X_l = 0.143$ marked as a dashed vertical line; note the maximum of X_l in the liquid phase denotes composition inversion as detailed in the text. (ii) Simulation results for $P(\phi_l)$ and $P(\phi_s)$ in the vapor and liquid phases for values of c_p/c_p^* shown in the key. Orange data denote small particles and blue data denote large particles. (iii) Schematic phase diagram. (a–c) refer to state points obtained in experiment depicted in Fig. 1. Squares are gels, triangles are liquid-vapour coexistence, and circles are one-phase fluid. Simulation results for volume fractions of coexisting phases are given by pale blue and orange lines.

of the small particles. This scenario is depicted schematically in Fig. 1(a1). A further possible interpretation of Fig. 1(a) is that liquid-liquid demixing occurred [Fig. 1(a2)] and two colloidal liquid phases coexist with the third, polymer-rich colloidal vapor, as indicated by the dashed lines in Fig. 1(a) inset. However, if such type II behaviour occurs, it is curious that the small particles subsequently remix with the large ones in a dense phase at larger polymer concentration c_p/c_p^* , as seen in Figs. 1(b) and 1(b1).

C. Results from simulation

To help resolve which scenario applies, we appeal to our Grand Canonical Monte Carlo simulation studies of the generalized Asakura-Oosawa model. Starting from the one-phase regime, the polymer reservoir concentration c_p^r was increased following the experimental isochore until the systems entered the coexistence region. This is indicated by the appearance of a double-peaked structure in the probability distribution of the fluctuating order parameter (which we take as the total volume fraction $\phi_{\text{tot}} = \phi_l + \phi_s$), as shown in Fig. 5(i). One of these peaks is at very low values of ϕ_{tot} , while the other is at a high value, indicating that the transition is vapor-liquid-like in character. We have followed the transition to large c_p^r where the liquid becomes very dense but see no sign of a splitting of the liquid peak, which would indicate liquid-liquid demixing, i.e., type II behavior. At higher densities, it becomes difficult to sample the liquid sufficiently in our simulations.

Thus, the simulations indicate that only a single vapor-liquid transition occurs, implying type I behavior. Moreover, they reveal that the puzzling differences between Figs. 1(a) and 1(b) (which suggests possible liquid-liquid demixing of colloids) might be attributed to the changing character of the fractionation as c_p^r is varied. Figure 5(b) plots the probability distributions $P(\phi_s)$ and $P(\phi_l)$ of the volume fractions of each species in the coexisting vapor and liquid phases for the various c_p^r studied. One observes from these distributions that the volume fraction difference of the large particles $\phi_l^{\text{liq}} - \phi_s^{\text{vap}}$

is very large even for small c_p^r approaching the critical point. This indicates that the vast majority of large particles occupy the liquid from the outset of phase separation. On increasing c_p^r , this difference grows further until, at the largest c_p^r studied, almost no large particles occupy the vapor. With regard to the small particles, at low values of c_p^r , ϕ_s^{liq} exceeds ϕ_s^{vap} , only slightly; i.e., there is initially only weak fractionation of the small particles upon phase separation; however, as c_p^r increases, $\phi_s^{\text{liq}} - \phi_s^{\text{vap}}$ grows strongly, indicating that the small particles migrate progressively from the vapor to the liquid. Figure 5(iii) summarises the phase behaviour as determined by experiment and simulation. Overall, there is good agreement.

D. Composition inversion

An interesting corollary of the fractionation behavior is that the concentration of large particles X_l in the liquid phase exhibits an unusual back-bending; i.e., as c_p^r increases, a maximum of X_l occurs [see the phase diagram in the inset of Fig. 5(i)]. We term this behavior *composition inversion*. It appears not to have been recognized previously in studies of binary mixtures.

The fractionation scenario revealed by the simulations can explain the differences in the images of Figs. 1(a) and 1(b). Figure 6(a) shows that for weak quenching and early times (before sedimentation), the large particles accumulate in the liquid phase, while the smaller are more homogeneously distributed. This can be seen by separating the fluorescent channels to reveal the spatial distributions of the individual species [Figs. 6(b) and 6(c)]. At larger quench depths, Figs. 6(d)–6(f), small particles follow the large particles in their spatial variation in density. In other words, the liquid phase is rich in both the colloid species.

E. Near-critical fluctuations

At the vapor-liquid critical point, one expects the system to display self-similar spatial density fluctuations on all

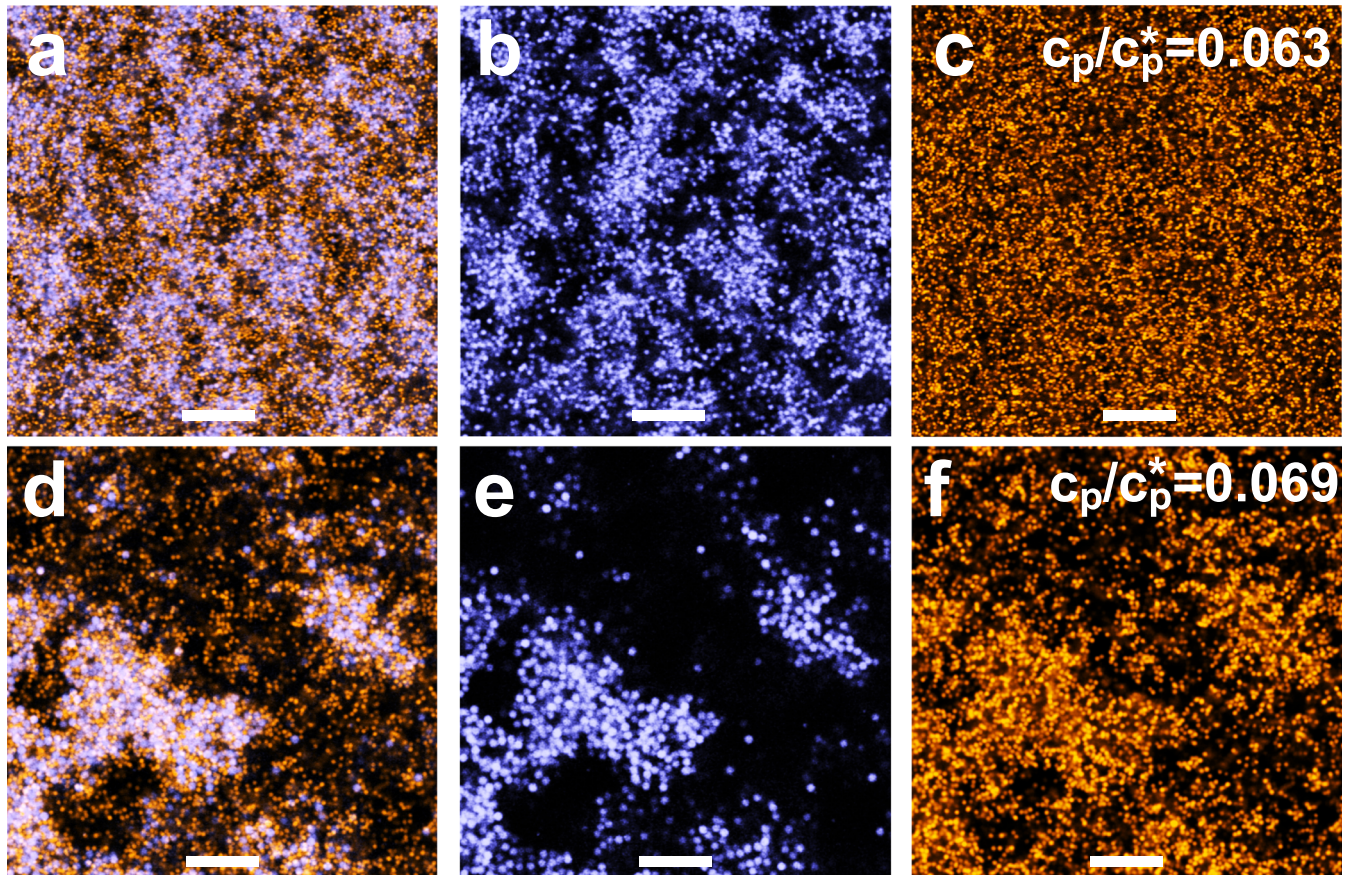


FIG. 6. Confocal images shortly after commencement of phase separation. The mixture [left panels (a) and (d)] is separated into the contributions from large particles [blue, middle panel (b) and (e)] and small particles [orange, right panel (c) and (f)]. [(a)–(c)], top row $c_p/c_p^* = 0.063$; [(d)–(f)], bottom row $c_p/c_p^* = 0.069$. Scale bars denote $25 \mu\text{m}$.

length scales. By reference to our simulations, the experimental path enters the coexistence region slightly on the vapor side of the critical point. The presence of density fluctuations on many length scales, as observed in Fig. 6 for a state point just inside the coexistence region, is therefore a reflection of the proximity to criticality. However, fractionation also affects the near-critical region: Principally, it is the large particles that partake in these fluctuations—the small ones are more homogeneously distributed. We have quantified this effect in both the experiments and the simulations by accumulating the probability distributions $P(\phi_s)$ and $P(\phi_l)$.

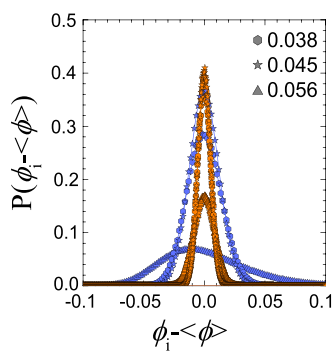


FIG. 7. Simulation results for $P(\phi_l)$ and $P(\phi_s)$ in the one-phase fluid on the experimental isochores for three values of c_p/c_p^* . Orange data denote small particles $i = s$ and blue data denote large particle $i = l$.

The analysis of volume fraction fluctuations for the individual species in the experiments was obtained by plotting a histogram of the volume fractions obtained via (1), sampled over square regions of side $7.0\sigma_l$. This differs from the simulation analysis that obtains the distribution of the fluctuating species volume fractions on the scale of the cubic simulation box. Because of the limited axial resolution of the microscope, we do not define 3D cubes very accurately at this length scale.

Figure 7 presents our simulation results on the critical isochores that shows that $P(\phi_s)$ is essentially Gaussian, while

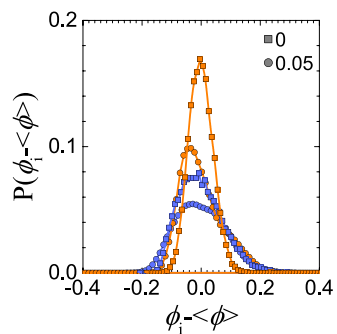


FIG. 8. Probability distributions of volume fraction $P(\phi_l)$ and $P(\phi_s)$ in experiments for two values of c_p/c_p^* . Orange data denote small particles $i = s$ and blue data denote large particles $i = l$. Note that the methodology for the experiments leads to quantitatively different distributions from simulation.

for the state closest to the critical point ($c_p/c_p^* = 0.056$) (blue triangles), $P(\phi_l)$ is non-Gaussian, with a distinct tail extending to higher values of ϕ_l , i.e., towards the critical point. Similar behaviour is found in the experiments (Fig. 8). These results suggest that the fluctuations in the two species are different in their sensitivity to deviations from criticality: the large particles with their stronger interparticle attractions respond first to approaching criticality, whereas the small particles with their weaker attractions only do so much closer to the critical point than we approach here.

IV. CONCLUSIONS

Using particle-resolved studies and bespoke Monte Carlo simulation, we have investigated the phase behavior of a simple ternary mixture of two colloidal and one polymer species. We have recast this ternary system as a binary colloid mixture, with effective interactions between the particles obtained by integrating out the polymer degrees of freedom. The current theoretical understanding of such mixtures is limited. Here, we see that adding a second colloidal species introduces a remarkable level of complexity into a well-understood system. Although a superficial inspection of Fig. 1 suggests that colloid liquid-liquid demixing may occur, our simulations show that this is illusory. Rather, strong fractionation of the large particles occurs and there is only a vapor-liquid-type separation. Thus, our combined experimental and computational approach resolves the intriguing phase behaviour of this simple mixture.

We find that the character of this vapor-liquid transition is much richer than that in the systems with one colloidal species due to multiple interaction ranges and strengths. At shallow quenches, the larger particles strongly prefer the liquid phase, while the smaller ones show only a weak preference—a phenomenon that can give the appearance of liquid-liquid demixing. However, for deeper quenches, the small particles migrate strongly to the liquid, reducing the concentration of the large particles and leading to composition inversion, i.e., a maximum in the concentration of large particles in the liquid phase. For the deepest quenches, a gel forms. Our study also shows that while criticality is a collective phenomenon of the mixture, for slightly off-critical conditions, density fluctuations are dominated by the larger colloids, while the smaller species behave somewhat as “spectators.” In other words, criticality and phase separation are driven predominantly by the larger particles. Given the basic nature of this system, we expect that this behavior may be found to apply widely in materials and formulations that are based on mixtures of colloids and polymers, such as cosmetics, foods, and pesticides.

ACKNOWLEDGMENTS

This work was supported jointly by Bayer CropScience AG and the UK Engineering and Physical Sciences Research Council through the award of an Industrial CASE award to I.Z. C.P.R. acknowledges the Royal Society for financial support and EPSRC Grant Code No. EP/H022333/1 for

provision of equipment used in this work, and the European Research Council under the FP7/ERC Grant Agreement No. 617266 and Kyoto University SPIRITS fund. R.P. acknowledges the Development and Promotion of Science and Technology Talents Project (DPST) of Thailand. N.B.W. acknowledges EPSRC Grant Nos. EP/F047800 and EP/I036192. R.E. acknowledges support from the Leverhulme Trust under No. EM-2016-031. This research made use of the Balena High Performance Computing Service at the University of Bath.

- ¹J. S. Rowlinson and F. L. Swinton, *Liquids and Liquid Mixtures*, Butterworth Monographs in Chemistry (Butterworth Scientific, 1982).
- ²P. H. van Konynenburg and R. L. Scott, “Critical lines and phase equilibria in binary van der waals mixtures,” *Philos. Trans. R. Soc., A* **298**, 495 (1980).
- ³D. Frenkel, “Playing tricks with ‘designer atoms,’” *Science* **296**, 65–66 (2002).
- ⁴A. Ivlev, H. Loewen, G. E. Morfill, and C. P. Royall, *Complex Plasmas and Colloidal Dispersions: Particle-Resolved Studies of Classical Liquids and Solids* (World Scientific Publishing Co., Singapore Scientific, 2012).
- ⁵W. C. K. Poon, “The physics of a model colloid-polymer mixtures,” *J. Phys.: Condens. Matter* **14**, R859 (2002).
- ⁶H. N. W. Lekkerkerker and R. Tuinier, “Colloids and the depletion interaction,” in *Lecture Notes in Physics* (Springer, Berlin, 2011), Vol. 833.
- ⁷D. G. A. L. Aarts, M. Schmidt, and H. N. W. Lekkerkerker, “Direct observation of thermal capillary waves,” *Science* **304**, 847–850 (2004).
- ⁸C. P. Royall, D. G. A. L. Aarts, and H. Tanaka, “Bridging length scales in colloidal liquids and interfaces from near-critical divergence to single particles,” *Nat. Phys.* **3**, 636–640 (2007).
- ⁹M. Leocmach, R. C. Royall, and H. Tanaka, “Novel zone formation due to interplay between sedimentation and phase ordering,” *Europhys. Lett.* **89**, 38006 (2010).
- ¹⁰J. Zhou, J. van Duijneveldt, and B. Vincent, “Two-stage phase separation in ternary colloid-polymer mixtures,” *Phys. Chem. Chem. Phys.* **13**, 110–113 (2011).
- ¹¹J. Zhou, J. van Duijneveldt, and B. Vincent, “Phase separation in mixtures of two sizes of silica particles dispersed in DMF on the addition of polystyrene,” *Mol. Phys.* **109**, 1187–1194 (2011).
- ¹²R. Pandey and J. C. Conrad, “Dynamics of confined depletion mixtures of polymers and bidispersed colloids,” *Soft Matter* **9**, 10617–10626 (2013).
- ¹³M. Schmidt, M. Dijkstra, and J.-P. Hansen, “Floating liquid phase in sedimenting colloid-polymer mixtures,” *Phys. Rev. Lett.* **93**, 088303 (2004).
- ¹⁴D. de las Heras, N. Doshi, T. Cosgrove, J. Phipps, D. I. Gittins, J. S. van Duijneveldt, and M. Schmidt, “Floating nematic phase in colloidal platelet-sphere mixtures,” *Sci. Rep.* **2**, 789 (2012).
- ¹⁵D. de las Heras and M. Schmidt, “The phase stacking diagram of colloidal mixtures under gravity,” *Soft Matter* **9**, 8636 (2013).
- ¹⁶D. de las Heras and M. Schmidt, “Sedimentation stacking diagram of binary colloidal mixtures and bulk phases in the plane of chemical potentials,” *J. Phys.: Condens. Matter* **27**, 194115 (2015).
- ¹⁷H. N. W. Lekkerkerker, W. C.-K. Poon, P. N. Pusey, A. Stroobants, and P. B. Warren, “Phase behaviour of colloid + polymer mixtures,” *Europhys. Lett.* **20**, 559 (1992).
- ¹⁸R. Evans and L. Purnell, “A simple hard sphere model for mixtures of colloidal particles with added polymer,” M.S. thesis (University of Bristol, 2013).
- ¹⁹N. B. Wilding, “Accurate simulation estimates of phase behavior in ternary mixtures with prescribed composition,” *J. Stat. Phys.* **144**, 652–662 (2011).
- ²⁰S. Asakura and F. Oosawa, “On interaction between two bodies immersed in a solution of macromolecules,” *J. Chem. Phys.* **22**, 1255–1256 (1954).
- ²¹S. Asakura and F. Oosawa, “Interaction between particles suspended in solutions of macromolecules,” *J. Polym. Sci.* **33**, 183–192 (1958).

- ²²C. P. Royall, R. van Roij, and A. van Blaaderen, "Extended sedimentation profiles in charged colloids: The gravitational length, entropy, and electrostatics," *J. Phys.: Condens. Matter* **17**, 2315–2326 (2005).
- ²³C. P. Royall, A. A. Louis, and H. Tanaka, "Measuring colloidal interactions with confocal microscopy," *J. Chem. Phys.* **127**, 044507 (2007).
- ²⁴F. Lo Verso, R. L. C. Vink, D. Pini, and L. Reatto, "Critical behavior in colloid-polymer mixtures: Theory and simulation," *Phys. Rev. E* **73**, 061407 (2006).
- ²⁵A. Fortini, E. Sanz, and M. Dijkstra, "Crystallization and gelation in colloidal systems with short-ranged attractive interactions," *Phys. Rev. E* **78**, 041402 (2008).
- ²⁶S. Taylor, R. Evans, and C. P. Royall, "Temperature as an external field for colloid-polymer mixtures: 'quenching' by heating and 'melting' by cooling," *J. Phys.: Condens. Matter* **24**, 464128 (2012).
- ²⁷M. Dijkstra, J. M. Brader, and R. Evans, "Phase behaviour and structure of model colloid-polymer mixtures," *J. Phys.: Condens. Matter* **11**, 10079–10106 (1999).
- ²⁸P. G. Bolhuis, A. A. Louis, and J. P. Hansen, "Influence of polymer-excluded volume on the phase-behavior of colloid-polymer mixtures," *Phys. Rev. Lett.* **89**, 128302 (2002).
- ²⁹D. G. A. L. Aarts, R. Tuinier, and H. N. W. Lekkerkerker, "Phase behaviour of mixtures of colloidal spheres and excluded-volume polymer chains," *J. Phys.: Condens. Matter* **14**, 7551–7561 (2002).
- ³⁰A. A. Louis, P. G. Bolhuis, E. J. Meijer, and J. P. Hansen, "Polymer induced depletion potentials in polymer-colloid mixtures," *J. Chem. Phys.* **117**, 1893–1907 (2002).
- ³¹V. Krakoviack, J. P. Hansen, and A. A. Louis, "Influence of solvent quality on effective pair potentials between polymers in solution," *Phys. Rev. E* **67**, 041801 (2003).
- ³²A. Vrij, "Polymers at interfaces and the interactions in colloidal dispersions," *Pure Appl. Chem.* **48**, 471–483 (1976).
- ³³J. Taffs, A. Malins, S. R. Williams, and C. P. Royall, "A structural comparison of models of colloid-polymer mixtures," *J. Phys.: Condens. Matter* **22**, 104119 (2010).
- ³⁴N. B. Wilding and P. Sollich, "Phase behavior of polydisperse spheres: Simulation strategies and an application to the freezing transition," *J. Chem. Phys.* **133**, 224102 (2010).
- ³⁵M. Buzzacchi, P. Sollich, N. B. Wilding, and M. Müller, "Simulation estimates of cloud points of polydisperse fluids," *Phys. Rev. E* **73**, 046110 (2006).